# Magnetic anisotropy of ferromagnetic $Ga_{1-x}Mn_xAs_{1-y}P_y$ films with graded composition

Seul-Ki Bac,[1,2,*] Sanghoon Lee,[1,*] Xinyu Liu,[2] Malgorzata Dobrowolska,[2] Badih A. Assaf,[2] and Jacek K. Furdyna[2]
[1]*Department of Physics, Korea University, Seoul 02841, Republic of Korea*
[2]*Department of Physics, University of Notre Dame, Notre Dame, Indiana 46556, USA*

(Received 12 January 2021; revised 19 April 2021; accepted 13 May 2021; published 28 May 2021)

We have investigated magnetic anisotropy properties of ferromagnetic semiconductor $Ga_{1-x}Mn_xAs_{1-y}P_y$ films grown by molecular beam epitaxy on GaAs substrates with constant Mn content $x$ of 0.06 and with P content $y$ graded along the growth direction. Two samples were investigated, one with $y$ increasing in the growth direction from 0.03 to 0.24, the other with $y$ decreasing from 0.25 to 0.04. Such grading of phosphorus concentration leads to a continuous variation of strain, and thus of magnetic anisotropy in the film. Although the phosphorus mole fraction in the films was varied by nearly the same amount in both "forward"- and "reverse"-graded samples, their magnetic anisotropy properties are entirely different. Specifically, while the forward-graded specimen can be described in terms of three distinct magnetic layers in which the magnetic easy axes progress from in plane to out of plane as the phosphorus concentration increases, the reverse-graded sample shows only an out-of-plane anisotropy throughout the entire film. This implies that the initial conditions at the nucleation of sample growth determine the magnetic properties of the entire graded $Ga_{1-x}Mn_xAs_{1-y}P_y$ film.

DOI: 10.1103/PhysRevMaterials.5.054414

## I. INTRODUCTION

Over the past two decades, diluted magnetic semiconductor alloys $Ga_{1-x}Mn_xAs$ have received attention as promising candidates for spintronic applications [1,2]. It is now well established that ferromagnetism in these alloys originates from exchange interactions between the spins of magnetic ions and itinerant holes [3]. This spin-carrier interplay offers remarkable features, such as a strong dependence of the Curie temperature on carrier density and a strong sensitivity of magnetic anisotropy of these alloys to epitaxial strains related to the strain-dependent anisotropy of the valence band [3,4]. Usually, when the $Ga_{1-x}Mn_xAs$ layers are under compressive strain (as in the case when they are grown on GaAs substrates), this situation favors in-plane magnetization [5]. On the contrary, when the $Ga_{1-x}Mn_xAs$ layers are under tensile strain, the magnetization of the layer orients spontaneously perpendicular to the film plane, as in the case of $Ga_{1-x}Mn_xAs$ films grown on $Ga_{1-x}In_xAs$ buffer layers [6], or when a sufficient concentration of phosphorus is incorporated into the $Ga_{1-x}Mn_xAs$ lattice [7,8]. Thus, quaternary $Ga_{1-x}Mn_xAs_{1-y}P_y$ alloys provide a powerful approach for tailoring magnetocrystalline anisotropy by controlling the concentration of P in the film [9,10].

Interfacial effects have been ubiquitously employed to induce symmetry breaking and perform band engineering in semiconductors [11–13]. One method to introduce and enhance such interfacial effects utilizes a composition gradient during the synthesis of semiconductors to tune strain and band structure [14]. In the present work, we studied magnetic anisotropy in $Ga_{1-x}Mn_xAs_{1-y}P_y$ samples in which the concentration of P is graded along with the film thickness, with Mn concentration kept at a constant value of $x \approx 0.06$. In such films, the graded phosphorus concentration is expected to lead to a gradient of the energy gap (and thus of the hole concentration, which mediates the Mn-Mn exchange coupling) and a gradient of strain (and thus of magnetic anisotropy parameters). One can then expect in such graded specimens an entirely different magnetic behavior with ferromagnetic properties. In fact, in our earlier studies of such graded systems [15,16], some of the authors have already found a pronounced and unique asymmetry of domain walls with respect to their easy axes, suggesting the presence of Dzyaloshinskii-Moriya interactions and programmable magnetic bias effects.

Importantly, the variation of magnetic anisotropy in the graded film can realize a monolithic ferromagnetic structure comprised of multiple magnetic sublayers with in-plane and out-of-plane components of magnetization, which is a candidate system for field-free spin-orbit torque switching [17–19]. Detailed investigation of magnetic anisotropy in the graded $Ga_{1-x}Mn_xAs_{1-y}P_y$ films is also likely to shed light on the importance of initial nucleation mechanism during crystal growth, which is closely related to crystallinity, composition, and defect formation [20,21], and can thus provide fruitful information for optimizing structures for spintronic device applications.

## II. EXPERIMENT

Composition-graded $Ga_{1-x}Mn_xAs_{1-y}P_y$ samples were grown on GaAs (001) substrates in a Riber 32 molecular beam epitaxy (MBE) system. During the growth, wafers were rotated to achieve a homogeneous composition in the film plane. For grading the P concentration, the $As_2$/(Ga, Mn) flux ratio was kept constant at ~10 during the entire growth, while the

*Corresponding authors: sbac@nd.edu; slee3@korea.ac.kr

 

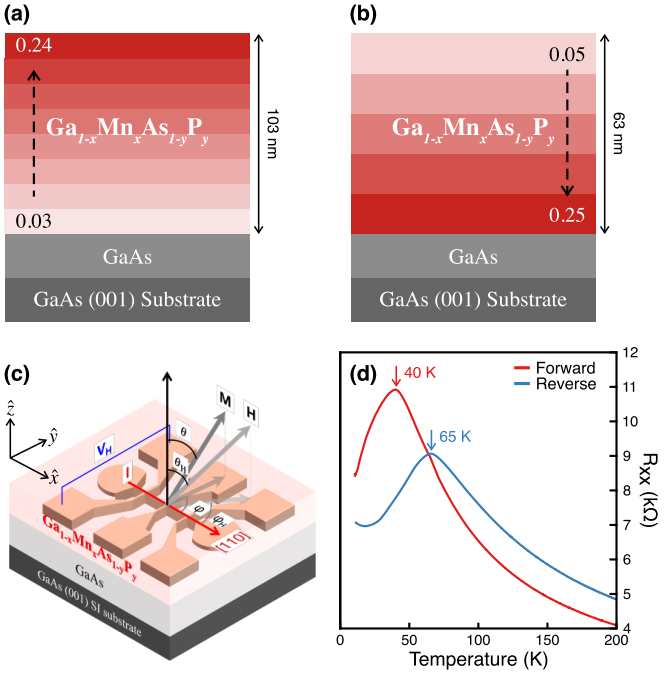


FIG. 1. Sketch of the structures for (a) forward- and (b) reverse-graded $Ga_{1-x}Mn_xAs_{1-y}P_y$ samples. Chemical compositions and the thicknesses shown in the figures for each sample were obtained by XRD measurements. (c) Schematic diagram of the Hall bar patterned on the graded $Ga_{1-x}Mn_xAs_{1-y}P_y$ film, indicating Hall voltage $V_H$, and directions of the current $\boldsymbol{I}$, magnetization $\boldsymbol{M}$, and external field $\boldsymbol{H}$. Current $\boldsymbol{I}$ flows along the [110] crystallographic direction. (d) Temperature dependences of resistances measured for the forward (red) and reverse (blue) samples.

$P_2/As_2$ ratio was gradually varied during the growth. In one sample (referred to as the "forward" sample), the $P_2/As_2$ flux ratio was increased from ∼0 to ∼1/2, and in the second sample (referred to as "reverse"), the $P_2/As_2$ ratio was reduced from ∼1/2 to ∼0 as the growth progressed. Such gradation of the flux ratio during growth resulted in $Ga_{1-x}Mn_xAs_{1-y}P_y$ films in which $y$ changes continuously either from 0.03 to 0.24 (the forward sample) or from 0.25 to 0.04 (the reverse sample) at a fixed value of $x \approx 0.06$. The atomic concentrations in both samples were examined by high-resolution x-ray diffraction (XRD) measurements, as described in Ref. [16]. The thicknesses of the forward and reverse samples were determined by the XRD data (see Fig. S1 in the Supplemental Material [22]) as 103 ± 1.8 nm and 63 ± 1.1 nm, respectively. Despite the variation of phosphorous concentrations, both samples were fully strained with no detectable relaxation (see Fig. S2 in [22]). Schematic cross sections of the graded $Ga_{1-x}Mn_xAs_{1-y}P_y$ films used in this investigation are shown in Figs. 1(a) and 1(b).

For electrical transport measurements, Hall bars were patterned by photolithography and dry etching, with the long direction along with the [110] crystalline orientation. A schematic image of the Hall device is shown in Fig. 1(c). Directions of the applied magnetic field and of magnetization in the films are indicated by angles $(\varphi_H, \theta_H)$ and $(\varphi, \theta)$, respectively, with the polar angles $\theta_H$ and $\theta$ measured from the [001] crystallographic direction, and the azimuthal angles $\varphi_H$ and $\varphi$ from the [110] direction (which is also the direction of the current), as shown in Fig. 1(c). The temperature dependence of resistance shown in Fig. 1(d) provides an estimate of Curie temperatures of the forward sample as 40 K and the reverse sample as 65 K. These agree well with the results obtained from the temperature dependence of $R_{xy}/R_{xx}^2$ extracted from Arrott plots (see Sec. II in [22]).

## III. RESULTS

In this study, we will use Hall effect measurements for determining the magnetic anisotropy of our graded specimens. We recall that the expression for Hall resistance in a ferromagnetic film is given by [1,23]

$$R_{xy} = R_0 \frac{H}{t}\cos\theta_H + R_S \frac{M}{t}\cos\theta + k\frac{M^2}{t}\sin^2\theta \sin 2\varphi, \quad (1)$$

where the first, second, and third terms on the right-hand side of Eq. (1) are the normal, anomalous, and planar Hall resistances, respectively. The terms $R_0$ and $R_S$ are the normal and anomalous Hall coefficients, $k$ is a constant related to the anisotropic magnetoresistance of the sample, and $M$ and $t$ are its magnetization and thickness. The anomalous and planar Hall resistances depend directly on the orientation of magnetization, which thus provide a convenient tool for determining the magnetic anisotropy of the film.

### A. Magnetic anisotropy of forward-graded sample

Field dependencies of the Hall resistances $R_{xy}$ of our graded $Ga_{1-x}Mn_xAs_{1-y}P_y$ samples measured at 10 K are shown in Fig. 2. Because the strain in the samples is graded, it is reasonable to expect that different sample sections may be characterized by in-plane and out-of-plane easy axes. This is clearly confirmed by the out-of-plane field scans of the forward sample shown in Fig. 2(b), in which a fraction of the $R_{xy}$ signal (of magnitude marked as $R_{\text{cent}}^{\text{OP}}$ in the figure) shows a distinct sharp hysteresis loop in the low-field region, indicating that a fraction of that sample has an out-of-plane easy axis. However, as the field increases beyond the central hysteresis, $R_{xy}$ continues to increase at a gradual rate. Since a portion of the sample with low phosphorus content is expected to have an in-plane easy axis, we ascribe the observed gradual increase of $R_{xy}$ to magnetization from that portion being "forced" normal to the sample plane by the out-of-plane field until the entire magnetization of the graded film aligns with the applied out-of-plane field, thus providing a measure of total magnetization, marked in Fig. 2(b) as $R_{\text{tot}}^{\text{OP}}$.

Figure 2(a) shows $R_{xy}$ for the forward sample obtained with the applied field scanned in the film plane (in this case at $\theta_H = 90°$, $\varphi_H \sim 100°$), showing a two-step switching behavior that is typically observed in planar Hall effect (PHE) measurements on the $Ga_{1-x}Mn_xAs$ films with two in-plane magnetic easy axes [24]. Importantly, however, the present results also show a small vertical shift between the up and down sweeps of the field, marked as $R_{\text{asym}}^{\text{IP}}$ in Fig. 2(a). Such a vertical shift of Hall resistance cannot be caused by the in-plane magnetic anisotropy of the layer and must be ascribed to a small contribution from the anomalous Hall effect (AHE) [25,26]. This can be explained by the fact that, although the

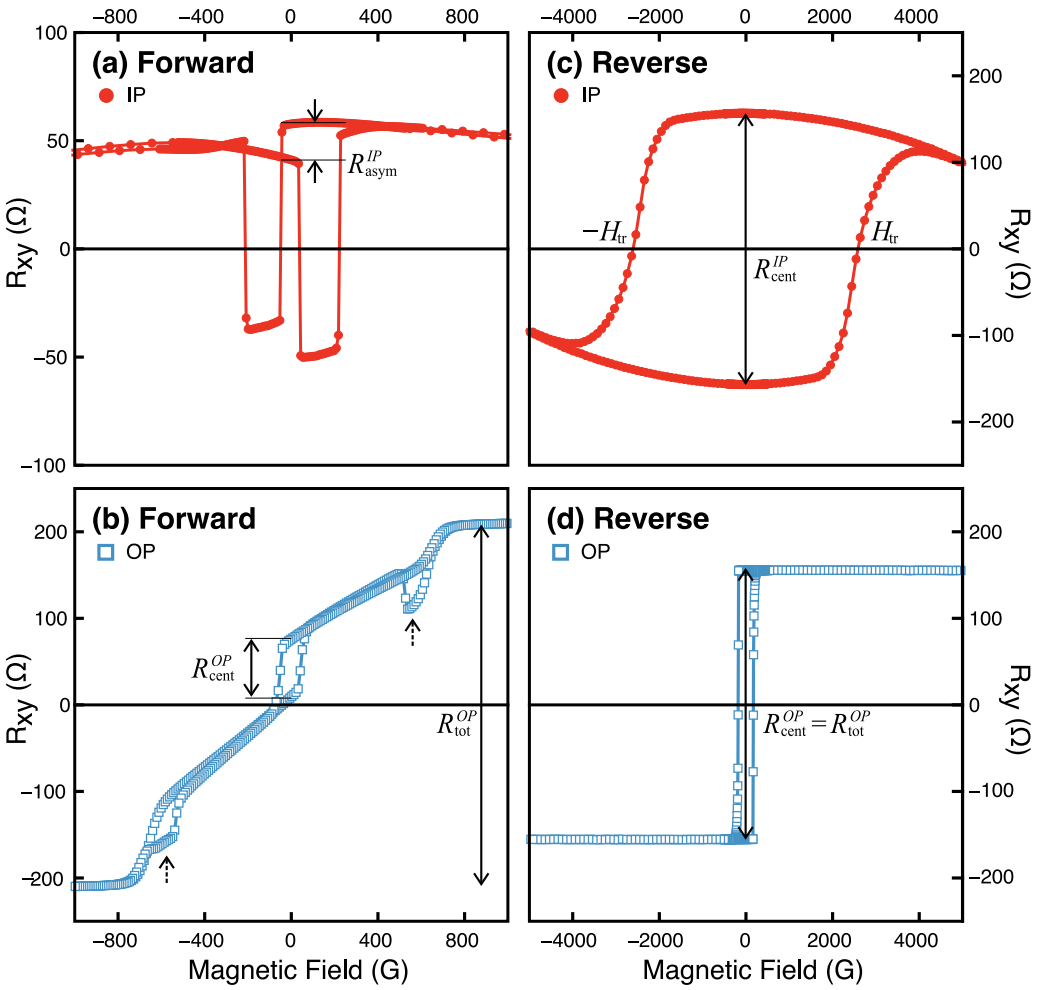


FIG. 2. Hall resistance $R_{xy}$ obtained by sweeping magnetic field in-plane (top row) and out-of-plane (bottom row) for forward (a),(b) and reverse (c),(d) samples at 10 K. $R^{IP}_{asym}$ and $R^{OP}_{cent}$ are differences of Hall resistance at zero field between up- and down-field scans in in-plane and out-of-plane data. $R^{OP}_{tot}$ represents a maximum change of the anomalous Hall resistance for out-of-plane field scan. $H_{tr}$ in (c) indicate transition fields in in-plane field scan for the reverse sample.

data in Fig. 2(a) are obtained with the field applied in the film plane, a slight misalignment of that field with the layer plane is inevitable, resulting in the presence of a weak but finite out-of-plane field component. Such an out-of-plane component of the applied field will then align the magnetization from the sample fraction having an out-of-plane easy axis [as identified in our discussion of Fig. 2(b)] normal to the film, resulting in the AHE contribution to $R_{xy}$, and thus in the observed shift marked as $R^{IP}_{asym}$. The two features observed around 600 G in Fig. 2(b) can thus be understood as resulting from such slight field misalignment, which introduces an admixture of PHE into the $R_{xy}$ data in Fig. 2(b), and thus an admixture of the steps associated with in-plane reorientations of magnetization seen in Fig. 2(a). Note, however, that the steps corresponding to these reorientations in Fig. 2(b) occur at fields much higher than in Fig. 2(a), since now a much higher field must be applied before the in-plane field component reaches the value required for such reorientations. The misalignment angle can be estimated from the difference of switching fields for the two measurements shown in Figs. 2(c) and 2(d), which give 4° as the upper end of the deviation angle.

Having established the origin of the asymmetry marked as $R^{IP}_{asym}$ in Fig. 2(a), and defining $R^{OP}_{cent}$ and $R^{OP}_{tot}$ in Fig. 2(b) that indicate, respectively, the contributions to AHE of the magnetization of the layer with an out-of-plane easy axis and the total (i.e., saturated) magnetization, we can now estimate the fractions of the forward sample characterized by in-plane and out-of-plane easy axes. In the out-of-plane measurements shown in Fig. 2(b), the ratio of $R^{OP}_{cent}/R^{OP}_{tot}$, indicating the fraction of the sample with an out-of-plane easy axis to the total sample magnetization, is approximately 20%. Similarly, the contribution of the out-of-plane magnetization to the planar Hall resistance shown in Fig. 2(a) can be calculated from $R^{IP}_{asym}$, since, as argued above, that represents the AHE contribution to $R_{xy}$ in the in-plane measurement. The value of $R^{IP}_{asym}/R^{OP}_{tot} \approx 0.1$, indicating that approximately 10% of the sample layer has out-of-plane magnetization at zero field.

Importantly, there is a factor of ~0.1 difference between the ratios $R^{IP}_{asym}/R^{OP}_{tot}$ obtained from the in-plane data in Fig. 2(a) and $R^{OP}_{cent}/R^{OP}_{tot}$ obtained from the out-of-plane data from Fig. 2(b), both indicating the fraction of the sample with out-of-plane magnetization. This implies that in the

forward-graded sample, there also is an intermediate magnetic layer having both in-plane and out-of-plane magnetic easy axes [27]. That is, the magnetization of such intermediate layer will contribute to $R_{\rm cent}^{\rm OP}$ observed in the vertical field sweep in Fig. 2(b) but will not contribute to $R_{\rm asym}^{\rm IP}$ observed in the in-plane field scans shown in Fig. 2(a). From these results, we argue that the forward sample consists of *three* regions, one with a robust in-plane easy axis, one with a robust out-of-plane easy axis, and one intermediate layer whose magnetization aligns in-plane when the field is applied in plane, and out of plane when the field is out of plane. Quantitatively, our results then indicate that nearly 10% of the sample (corresponding to the P-rich region near the top of the layer, where tensile strain is the greatest) has a robust out-of-plane easy axis; the bottom 80% of the sample (i.e., the region with lower P concentration, where either compressive or low tensile strain occurs) has a robust in-plane easy axis; and the remaining 10% of the sample (presumed to be between these two regions) corresponds to the intermediate layer.

### B. Magnetic anisotropy of reverse-graded sample

In contrast to the forward sample, the case of the reverse-grown specimen shows a single magnetic anisotropy, regardless of the applied magnetic field directions, as shown in Figs. 2(c) and 2(d). The out-of-plane data in Fig. 2(d) clearly show an abrupt square single hysteresis with a minimal coercive field, indicating a robust out-of-plane easy axis. The in-plane measurement data seen in Fig. 2(c) also shows a single hysteresis, but the hysteresis is much broader, which requires explanation. Since there is no in-plane easy axis in the case of this sample, to understand the width and shape of the hysteresis observed in the in-plane measurements, we again must invoke the unintended slight tilt of the applied field, $H_{\rm ex}$, relative to the sample plane. The transition condition for the in-plane scan is $|H_z| = |H_{\rm ex}\sin\delta| \approx |H_c|$, where $H_z$ is a small vertical component of $H_{\rm ex}$ due to the slight misalignment between $H_{\rm ex}$ and the sample plane, and $H_c$ is the coercive field of the sample. Since the field $H_{\rm ex}$ is applied near the film plane and the angle $\delta$ is caused by the slight misalignment, the value of $\delta$ is very small. This requires a much larger $H_{\rm ex}$ in the in-plane measurement than $H_c$ observed in out-of-plane measurements to achieve magnetization reversal. Importantly, the magnitudes of the Hall resistance at zero field are the same for the in-plane and out-of-plane field scans (i.e., $R_{\rm cent}^{\rm IP}$ and $R_{\rm cent}^{\rm OP}$), as seen in Figs. 2(c) and 2(d), clearly indicating that the entire sample behaves as a single magnetic domain with strong single out-of-plane anisotropy.

### C. Magnetic anisotropy parameters of graded samples

As shown in earlier studies [28–30], a numerical description of the magnetic anisotropy of a magnetic film can be conveniently determined by measuring and analyzing the angular dependence of the Hall resistance. We now follow this procedure to obtain the values of magnetic anisotropy parameters for our forward- and reverse-graded samples. The solid-circle and open-square data in Fig. 3 show the Hall resistance results obtained by rotating the magnetic field with a fixed magnitude in the (001) and (110) planes, respectively. In the case of the reverse sample [see Fig. 3(b)], only the

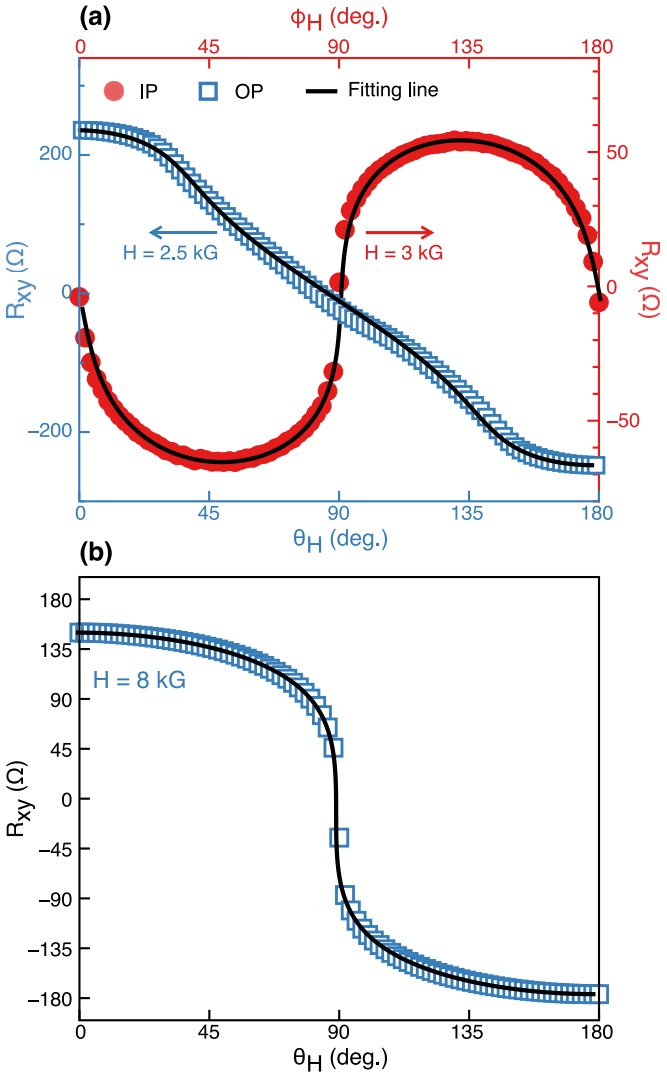


FIG. 3. Angular dependence of Hall resistance measured at 5 K for (a) forward and (b) reverse samples. Solid circles represent data obtained by rotating the field within the film plane [i.e., the (001) plane, referred to as *xy* plane]; and open squares are obtained with field rotated out of plane [i.e., in the (110) plane, referred to as *yz* plane]. Black solid curves are fitting results obtained using magnetic free energy anisotropy field parameters discussed in the text.

out-of-plane angular dependence data [i.e., only for the field rotated in the (110) plane] were measured since there is no in-plane magnetic anisotropy in that sample. The strengths of the rotating magnetic fields were chosen to be sufficiently high to coherently rotate the magnetization of the films as the field is rotated.

The angular dependence of magnetization (and therefore of $R_{xy}$) can then be understood in terms of magnetic free energy $E$, given by [28,29]

$$\frac{E}{M} = -\frac{1}{16}H_{4\parallel}(3-\cos 4\varphi)\sin^2\theta - \frac{1}{4}H_{4\perp}\cos^4\theta - \frac{1}{2}H_{2\parallel}\sin^2\theta\sin^2\varphi + \frac{1}{2}(4\pi M - H_{2\perp})\cos^2\theta - H[\cos\theta\cos\theta_H + \sin\theta\sin\theta_H\cos(\varphi-\varphi_H)], \quad (2)$$

TABLE I. Magnetic anisotropy components of graded $Ga_{1-x}Mn_xAs_{1-y}P_y$ samples.

| | $H_{4\parallel}$(G) | $H_{4\perp}$(G) | $H_{2\parallel}$ | $H_{2\perp}$(G) |
|---|---|---|---|---|
| Forward | 577.3 | 1600 | −396.5 | −1164 |
| Reverse | – | 713 | – | 8008 |

where $H_{4\parallel}$ and $H_{4\perp}$ are the in-plane and out-of-plane components of the cubic anisotropy field, and $H_{2\parallel}$ and $H_{2\perp}$ are the in-plane and the out-of-plane components of the uniaxial anisotropy field. Since the magnetization of the film follows the free energy minima as the magnetization rotates, and the value of the Hall resistances depends directly on the direction of the magnetization, the angular dependence of the Hall resistances can be fitted by using the magnetic anisotropy fields shown in Eq. (2) as fitting parameters. For fitting the values, we adapted the magnetization value of 32 emu/cm$^3$ obtained in an earlier study carried out on the samples with a similar Mn concentration [31]. The fitting process used here is described in detail in Ref. [30], and the results of the fitting are shown in Fig. 3.

The magnetic anisotropy parameters obtained by this analysis are summarized in Table I. Note that transport measurements probe the entire sample, rather than each of the layers separately. The magnetic anisotropy parameters obtained from these measurements thus represent the sample as a whole, even though the forward sample consists of different sublayers having different magnetic free energies.

Three-dimensional (3D) diagrams of magnetic free energy constructed using the fitting parameters in Table I are shown in Figs. 4(a) and 4(b). Figure 4(b) clearly shows that the reverse sample is described by a simple anisotropy determined by only one vertical easy axis. In sharp contrast, the case of the forward sample is much more complex, consisting of coexisting distinct in-plane and out-of-plane anisotropies shown in Fig. 4(a) that arise from contributions of the three sublayers comprising this sample, as discussed earlier. We plot the *xy* (i.e., the film plane) and the *yz* (i.e., the out of plane) cross-sectional profiles of magnetic free energy for the forward sample in Figs. 4(c) and 4(d). Figure 4(c) represents the in-plane anisotropy of the forward sample, corresponding to the bottom and the intermediate sublayers. The twofold symmetry of the in-plane anisotropy imposed by the portion

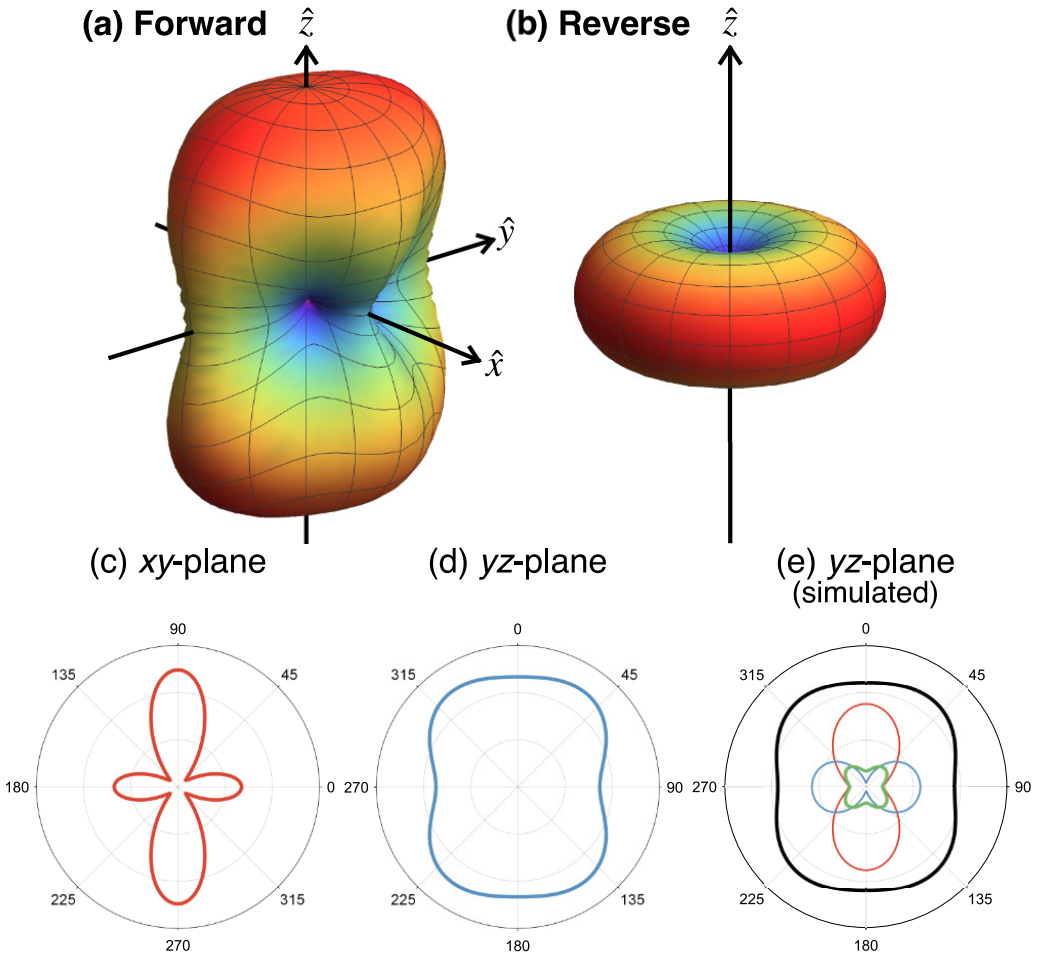


FIG. 4. Three-dimensional (3D) polar plots of magnetic free energy density for (a) forward and (b) reverse samples. Cross-sectional 2D plots for the *xy* plane and the *yz* plane for the forward sample are shown in panels (c) and (d), respectively. (e) The red, green, and blue lines represent magnetic anisotropies for the bottom, middle, and top sublayers of the forward sample, respectively. The black curve in (e) is the free energy contour obtained by summing magnetic anisotropy contributions of the three magnetic sublayers using the ratios obtained from Fig. 2.

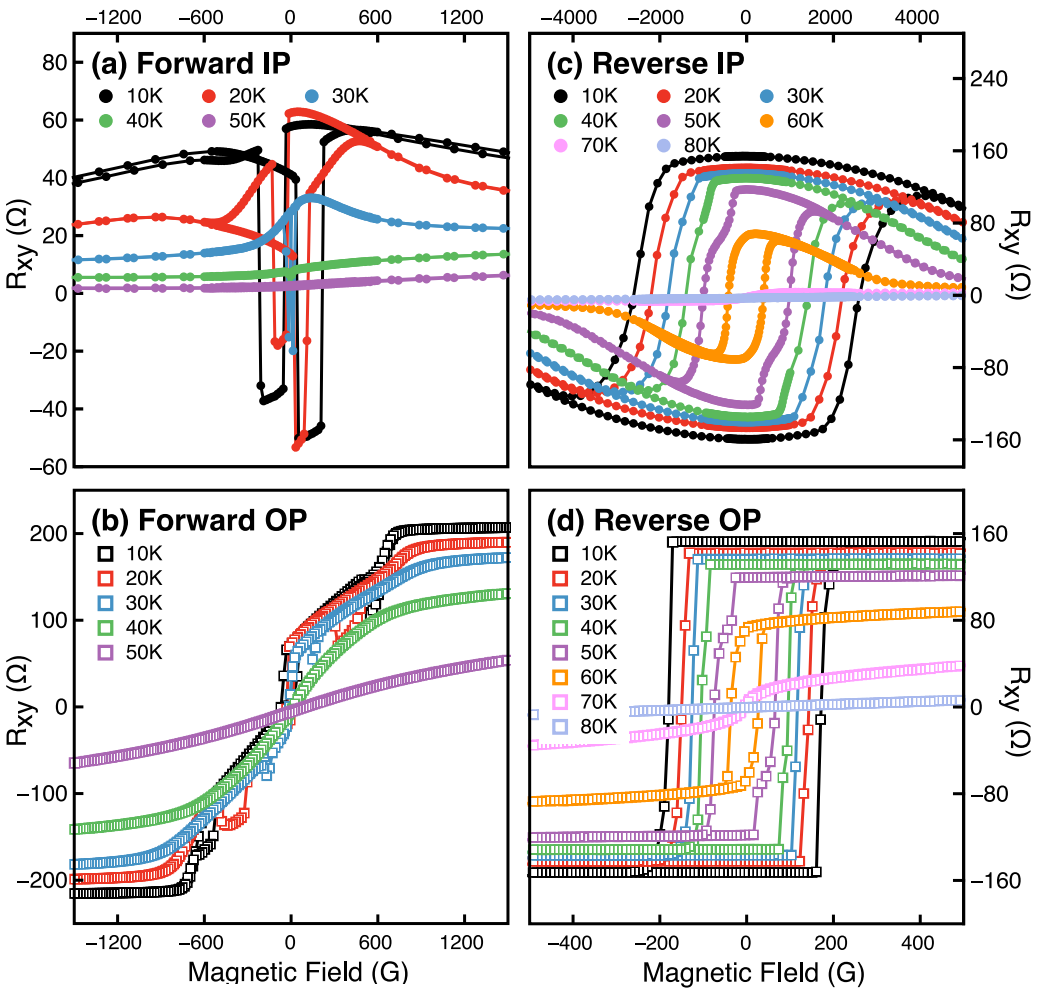


FIG. 5. Hall resistances $R_{xy}$ obtained by sweeping magnetic field along in-plane (top row) and out-of-plane (bottom row) directions for forward and reverse samples at several temperatures.

of the sample with in-plane easy axes is evident in the energy diagram in Fig. 4(c).

The origins of the vertical cross section (i.e., the *yz* plane diagram) of the forward sample shown in Fig. 4(d) are more complex in that the energy profile for that case involves contributions of the sublayers with the in-plane and the out-of-plane symmetries, along with that of the intermediate sublayer. Fortunately, the contributions from each of the sublayers can be inferred from the ratios of the perpendicular-to-total magnetization for each sublayer that have already been obtained from Fig. 2. We recall the weight factors of 0.80, 0.10, and 0.10 obtained from the analysis of Fig. 2 for the bottom (in-plane easy axis), intermediate (easy axes both in-plane and out-of-plane), and top sublayers (easy axis in out-of-plane direction), respectively. The contributions from each of the sublayers to the total anisotropy are plotted as red, green, and blue curves in Fig. 4(e). The sum of all three anisotropy diagrams, plotted as a black line in Fig. 4(e), very nicely reproduces the energy contour obtained experimentally for the *yz* plane shown in Fig. 4(d).

### D. Temperature dependence of magnetic anisotropy of graded samples

To obtain additional insight into the magnetic anisotropy of the graded $Ga_{1-x}Mn_xAs_{1-y}P_y$ samples, we have also studied the dependencies of the Hall resistances on the temperature in our two specimens by sweeping the magnetic field both in plane and out of plane at several temperatures, as shown in Fig. 5. In the case of the forward sample [Figs. 5(a) and 5(b)], one can clearly see that the magnitude of the Hall resistances for the in-plane and out-of-plane field scans decrease very rapidly with increasing temperature, and nearly disappear at 40 K, close to the Curie temperature of the forward sample.

The reverse sample also shows a systematic decrease of the amplitude and the width of the hysteresis in both in-plane and out-of-plane measurements as temperature increases [see Figs. 5(c) and 5(d)]. This behavior is typical for a ferromagnetic layer with perpendicular anisotropy. However, note that a two-step transition behavior becomes evident in these measurements at 50 K and disappears again above 60 K in Figs. 5(c) and 5(d). We interpret this as an indication that

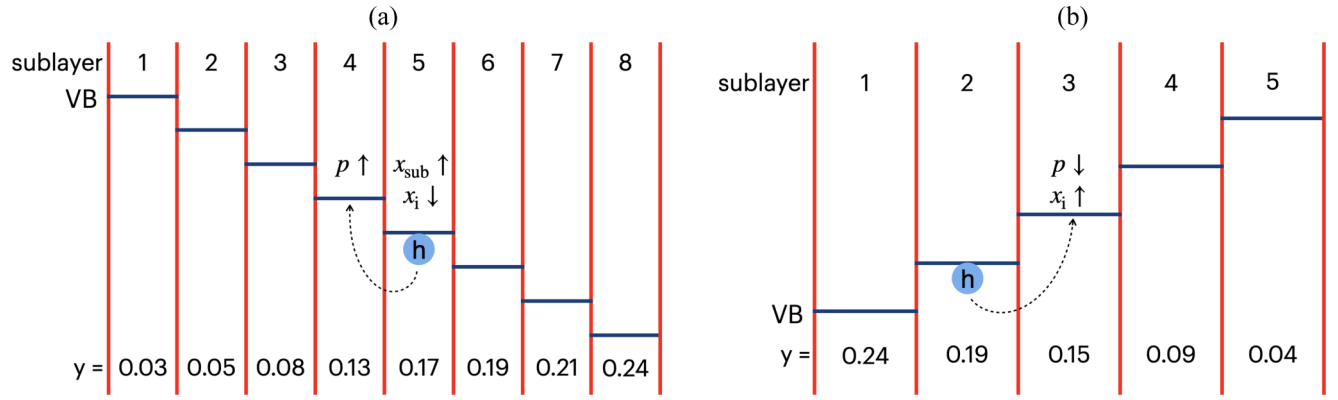


FIG. 6. Schematic band structure of forward (a) and reverse (b) samples. Blue lines mark each top of the valence band (VB) in successive sublayers. Chemical compositions shown in the figures for each sublayer were obtained by XRD measurements.

the reverse sample is also divided into two magnetically different regions with out-of-plane anisotropy but with different Curie temperatures. That is, even though the reverse sample shows a simple single-domain behavior at low temperature, the coercive field in different fractions of the layer exhibits different rates of decrease with the temperature (presumably due to different phosphorus content due to grading), the difference becoming conspicuous around 40 K. However, since one fraction of the film reaches the Curie temperature first, above 60 K, the behavior returns to a single-hysteresis behavior.

## IV. DISCUSSION

The results described above are rather unexpected. First, since the gradation of phosphorus in both samples is very similar and the strain is not relaxed in the two samples, one would expect them to have approximately similar distributions of in-plane and out-of-plane magnetizations, albeit along opposite directions. And second, both samples contain more layers with tensile than compressive strain, and thus one would expect that both will have a larger fraction of sublayers with perpendicular than with in-plane anisotropy. Surprisingly, however, neither of these expectations is true. As has been shown, the forward sample is dominated in a ratio of about 8:1 by magnetic in-plane anisotropy, while in the reverse sample the effect of in-plane anisotropy is entirely eliminated. In the following discussion, we attempt to explain these unexpected results.

Let us first consider the forward sample. We know that the top of the valence band of GaP lies approximately 400 meV lower in the energy than in GaMnAs. We therefore expect that as the phosphorus concentration is increased in each additional layer of our graded GaMnAsP sample, the top of the valence band will move progressively downward by a few meV relative to the preceding layer, as schematically indicated in Fig. 6(a). This will lead to interesting growth dynamics in such a graded system, as discussed below, and will have an important effect on the properties of the resulting specimen.

Consider the first ($y = 0.03$) sublayer 1 in Fig. 6(a). When it is grown, it will have a certain concentration $x_{\mathrm{sub}}$ of Mn ions substitutionally occupying Ga sites, and a certain concentration of Mn interstitials $x_{\mathrm{i}}$ characteristic for the growth conditions used. We recall that the substitutional incorporation of Mn at Ga sites is limited by the Fermi energy, as discussed in Yu *et al.* [32], resulting in the formation of Mn interstitials when the concentration of holes due to $x_{\mathrm{sub}}$ exceeds a certain limit. Now, as we deposit sublayer 2 [$y = 0.05$ in Fig. 6(a)] on sublayer 1, the small but finite band offset between the two layers will become important. Like in the modulation doping experiments of Wojtowicz *et al.* [33], some holes will be siphoned off into sublayer 1 due to the band offset between the layers. This lowers the Fermi energy in sublayer 2, allowing $x_{\mathrm{sub}}$ to increase, and reducing $x_{\mathrm{i}}$ formed in this layer. We now recall that the number of active magnetic moments in a given layer is proportional to $x_{\mathrm{eff}} = x_{\mathrm{sub}} - x_{\mathrm{i}}$, and the number of holes is determined by $x_p = x_{\mathrm{sub}} - 2x_{\mathrm{i}}$ [21], indicating that magnetization $M$ of sublayer 2 will be more robust than in sublayer 1 due to the increase in $x_{\mathrm{sub}}$ and the reduction of $x_{\mathrm{i}}$. Similarly, as sublayer 3 is being grown, the holes produced by substitutional incorporation of Mn are siphoned off to the preceding layer(s), again allowing a higher substitutional and lower interstitial incorporation of Mn, and leading to a greater magnitude of $M$. We can now make the same argument for sublayers 4, 5, etc.: as each successive layer is grown, holes are drained off to the preceding layer(s), allowing the growing layer to end up with larger substitutional incorporation of Mn at Ga sites and consequently a lower concentration of the harmful mobile interstitials.

While this process would appear to lead to increased magnetization in successive layers, there are important tradeoffs that must be considered. As each new layer is grown, the holes themselves—of key importance to the ferromagnetism of the material—are drained off to layers grown earlier. It is likely that, as the number of layers already grown increases, the "sink" for these holes becomes increasingly more effective, in analogy to modulation doping experiments, where it was shown that the effect of a doped barrier in modulation doping is proportional to its width [34]. Additionally, in this case one needs to consider the effect of increasing phosphorus concentration on the magnetization in successive layers of the forward sample. It has been shown by Dong *et al.* [21] that increasing phosphorus concentration leads to increased localization of holes, which automatically reduces magnetization. Based on these tradeoffs, it appears likely that the center of gravity of magnetization in the multilayer would naturally occur somewhere in the middle layers. However, at this time,

we cannot meaningfully discuss just where in the multilayer this takes place.

This interpretation appears quite consistent with the data shown in Fig. 2, which indicate that the forward sample as a whole is described by 80–90% of in-plane magnetization. At first glance this behavior would be surprising, since not more than three layers of the sample correspond to strain conditions that favor in-plane magnetic anisotropy, while the remaining five layers favor perpendicular magnetization. However, the picture presented above explains this quite nicely, despite its qualitative nature. As new layers are grown, the concentration of holes in the lower layers (i.e., those favoring in-plane anisotropy) increases both through hole drainage from layers grown later and (except for sublayer 1) through a lower rate of formation of Mn interstitials. These processes result in a disproportional increase of magnetization in the lower layers, consistent with the observed anisotropy of magnetization.

We now consider the reverse sample, again starting with the first ($y = 0.24$) layer illustrated by Fig. 6(b). When it was grown, this layer had concentrations $x_{\text{sub}}$ and $x_{\text{i}}$ consistent with the low-temperature MBE growth conditions used, so that the effective Mn spin concentration in the layer is given by $x_{\text{eff}}$, and the hole concentration is proportional to $x_p$ defined earlier. When the second ($y = 0.19$) layer is deposited, because of the band offset shown in Fig. 6(b), some holes are siphoned from the first layer into this sublayer 2 as its growth takes place. (We notethat, in the forward sample, holes were drained away from the sample being grown. In the reverse case, they were siphoned into the growing sample.) This does not affect the interstitials in the first layer since that layer is already grown; but in sublayer 2, the presence of additional holes now inhibits Mn substitution at Ga sites, thus causing more interstitials to form. So, in sublayer 2, we now have a reduced number of active Mn moments and also significantly fewer holes formed (both due to the lower rate of formation of $x_{\text{sub}}$ and due to compensation by Mn interstitials $x_{\text{i}}$ whose rate of formation is increased). The same argument can now be applied to sublayers 3, 4, etc. So, as P decreases in successive layers, moving the top of the valence band to higher energy with each successive layer, more interstitials will form in the new layers, reducing substitutional incorporation of Mn, and thus successively reducing their magnetization. It must be emphasized that the deleterious effect of interstitials on magnetization is very strong, and can exceed the beneficial effect of holes entering the layer, as has been strikingly demonstrated in codoping experiments of Lee *et al.* [35], who showed that adding holes to GaMnAs by additional doping results (counterintuitively) in a reduction rather than an increase of magnetization. The large influx of holes into uppermost layers from the rest of the sample may thus prevent substitutional incorporation of Mn to such a degree that magnetization of those layers will be substantially reduced, or will even vanish altogether. As a result, the magnetization of the reverse graded sample is also dominated by the bottom layers, which in this case favor perpendicular magnetic anisotropy, consistent with the observed orientation of magnetization in this specimen.

## V. CONCLUSIONS

Magnetic anisotropy of $Ga_{1-x}Mn_xAs_{1-y}P_y$ samples with graded phosphorus concentration shows distinct differences between forward- and reverse-graded specimens, even though the P concentration $y$ varies over a similar range (i.e., from about $y \approx 0$ to $y \approx 0.25$) in both films. Most of the forward-graded sample is strongly dominated by in-plane easy axes of magnetization, while the reverse-graded specimen exhibits only out-of-plane magnetization. This indicates, surprisingly, that growth dynamics of graded the $Ga_{1-x}Mn_xAs_{1-y}P_y$ film predetermines the magnetic properties of the entire film, despite the graded composition profile of the sample. While these results by themselves already provide helpful information for engineering magnetic anisotropy in ferromagnetic $Ga_{1-x}Mn_xAs_{1-y}P_y$ films by gradual variation of the phosphorus content during growth, the observed behavior is quite unexpected and requires further study to understand its physical origins.

## ACKNOWLEDGMENTS

This research was supported by the Basic Science Research Program through the National Research Foundation of Korea (NRF) funded by the Ministry of Education (Grant No. 2018R1D1A1A02042965); by the Basic Science Research Program through the NRF of Korea (Grant No. 2021R1A2C1003338); by the Ministry of Science ICT (Grant No. 2018R1A4A1024157); by the NRF under the BK21 FOUR program at Korea University, Initiative for science frontiers on upcoming challenges; by Korea University Grant; and by National Science Foundation Grant No. DMR 1905277.

[1] H. Ohno, Science **281**, 951 (1998).
[2] T. Dietl and H. Ohno, Rev. Mod. Phys. **86**, 187 (2014).
[3] T. Dietl, H. Ohno, F. Matsukura, J. Cibert, and D. Ferrand, Science **287**, 1019 (2000).
[4] M. Abolfath, T. Jungwirth, J. Brum, and A. H. MacDonald, Phys. Rev. B **63**, 054418 (2001).
[5] M. Sawicki, F. Matsukura, A. Idziaszek, T. Dietl, G. M. Schott, C. Ruester, C. Gould, G. Karczewski, G. Schmidt, and L. W. Molenkamp, Phys. Rev. B **70**, 245325 (2004).
[6] A. Shen, H. Ohno, F. Matsukura, Y. Sugawara, N. Akiba, T. Kuroiwa, A. Oiwa, A. Endo, S. Katsumoto, and Y. Iye, J. Cryst. Growth **175-176**, 1069 (1997).
[7] H. Lee, J. Chang, P. Chongthanaphisut, S. Lee, S. Choi, S.-K. Bac, A. R. Nasir, S. Lee, A. Pardo, S. Dong, X. Li, X. Liu, J. K. Furdyna, and M. Dobrowolska, AIP Adv. **7**, 055809 (2017).
[8] J. Chang, S. Choi, K. Lee, S.-K. Bac, S. Choi, P. Chongthanaphisut, S. Lee, X. Liu, M. Dobrowolska, and J. K. Furdyna, J. Cryst. Growth **512**, 112 (2019).
[9] M. Cubukcu, H. J. von Bardeleben, K. Khazen, J. L. Cantin, O. Mauguin, L. Largeau, and A. Lemaître, Phys. Rev. B **81**, 041202(R) (2010).
[10] A. Lemaître, A. Miard, L. Travers, O. Mauguin, L. Largeau, C. Gourdon, V. Jeudy, M. Tran, and J.-M. George, Appl. Phys. Lett. **93**, 021123 (2008).

[11] M. L. Lee, E. A. Fitzgerald, M. T. Bulsara, M. T. Currie, and A. Lochtefeld, J. Appl. Phys. **97**, 011101 (2005).
[12] C.-Z. Ning, L. Dou, and P. Yang, Nat. Rev. Mater. **2**, 17070 (2017).
[13] A. Werpachowska and T. Dietl, Phys. Rev. B **82**, 085204 (2010).
[14] T. Gora and F. Williams, Phys. Rev. **177**, 1179 (1969).
[15] V. K. Vlasko-Vlasov, W. K. Kwok, S. Dong, X. Liu, M. Dobrowolska, and J. K. Furdyna, Phys. Rev. B **98**, 180411(R) (2018).
[16] S. Dong, Y.-L. Wang, S.-K. Bac, X. Liu, V. Vlasko-Vlasov, W.-K. Kwok, S. Rouvimov, S. Lee, M. Dobrowolska, and J. K. Furdyna, Phys. Rev. Mater. **3**, 074407 (2019).
[17] T. Niazi, M. Cormier, D. Lucot, L. Largeau, V. Jeudy, J. Cibert, and A. Lemaître, Appl. Phys. Lett. **102**, 122403 (2013).
[18] M. Cormier, V. Jeudy, T. Niazi, D. Lucot, M. Granada, J. Cibert, and A. Lemaître, Phys. Rev. B **90**, 174418 (2014).
[19] S.-H. C. Baek, V. P. Amin, Y.-W. Oh, G. Go, S.-J. Lee, G.-H. Lee, K.-J. Kim, M. D. Stiles, B.-G. Park, and K.-J. Lee, Nat. Mater. **17**, 509 (2018).
[20] K. M. Yu, W. Walukiewicz, T. Wojtowicz, W. L. Lim, X. Liu, U. Bindley, M. Dobrowolska, and J. K. Furdyna, Phys. Rev. B **68**, 041308(R) (2003).
[21] S. Dong, L. Riney, X. Liu, L. Guo, R.-K. Zheng, X. Li, S.-K. Bac, J. Kossut, M. Dobrowolska, B. Assaf, and J. K. Furdyna, Phys. Rev. Mater. **5**, 014402 (2021).
[22] See Supplemental Material at http://link.aps.org/supplemental/10.1103/PhysRevMaterials.5.054414 for a description of structural information and details of Arrott plot analysis.
[23] K. Okamoto, J. Magn. Magn. Mater. **35**, 353 (1983).
[24] H. X. Tang, S. Masmanidis, R. K. Kawakami, D. D. Awschalom, and M. L. Roukes, Nature (London) **431**, 52 (2004).
[25] W. L. Lim, X. Liu, K. Dziatkowski, Z. Ge, S. Shen, J. K. Furdyna, and M. Dobrowolska, Phys. Rev. B **74**, 045303 (2006).
[26] T. Yoo, S. Khym, S.-Y. Yea, S. Chung, S. Lee, X. Liu, and J. K. Furdyna, Appl. Phys. Lett. **95**, 202505 (2009).
[27] M. Yahyaoui, C. Testelin, C. Gourdon, and K. Boujdaria, J. Appl. Phys. **111**, 033902 (2012).
[28] M. Farle, Rep. Prog. Phys. **61**, 755 (1998).
[29] X. Liu, W. L. Lim, L. V. Titova, M. Dobrowolska, J. K. Furdyna, M. Kutrowski, and T. Wojtowicz, J. Appl. Phys. **98**, 063904 (2005).
[30] H. Son, S. Chung, S.-Y. Yea, S. Lee, X. Liu, and J. K. Furdyna, J. Appl. Phys. **103**, 07F313 (2008).
[31] X. Li, X. Liu, S. Dong, C. Gorsak, J. K. Furdyna, M. Dobrowolska, S.-K. Bac, S. Lee, and S. Rouvimov, J. Vac. Sci. Technol. B **36**, 02D104 (2018).
[32] K. M. Yu, W. Walukiewicz, T. Wojtowicz, I. Kuryliszyn, X. Liu, Y. Sasaki, and J. K. Furdyna, Phys. Rev. B **65**, 201303(R) (2002).
[33] T. Wojtowicz, W. L. Lim, X. Liu, M. Dobrowolska, J. K. Furdyna, K. M. Yu, W. Walukiewicz, I. Vurgaftman, and J. R. Meyer, Appl. Phys. Lett. **83**, 4220 (2003).
[34] K. M. Yu, T. Wojtowicz, W. Walukiewicz, X. Liu, and J. K. Furdyna, in *Semiconductors and Semimetals*, edited by E. R. Weber (Elsevier, 2008), pp. 89–133.
[35] S. Lee, S. J. Chung, I. S. Choi, S. U. Yuldeshev, H. Im, T. W. Kang, W.-L. Lim, Y. Sasaki, X. Liu, T. Wojtowicz, and J. K. Furdyna, J. Appl. Phys. **93**, 8307 (2003).